Heliyon 5 (2019) e02914

Contents lists available at ScienceDirect

Heliyon

journal homepage: www.cell.com/heliyon

Research article

Hemocompatibility and safety of the Carmat Total Artifical Heart hybrid membrane

Ulysse Richez [a,b,c], Hector De Castilla [c], Coralie L. Guerin [d,e], Nicolas Gendron [f], Giulia Luraghi [g], Marc Grimme [c], Wei Wu [g], Myriam Taverna [h], Piet Jansen [c], Christian Latremouille [i], Francesco Migliavacca [g], Gabriele Dubini [g], Antoine Capel [c], Alain Carpentier [i], David M. Smadja [f,*]

[a] Université de Paris, Innovative Therapies in Haemostasis, INSERM UMR-S1140, F-75006, Paris, France
[b] et Laboratoire de Recherches Biochirugicales (Fondation Carpentier), AH-HP, Georges Pompidou European Hospital, F-75015, Paris, France
[c] Carmat SA, Vélizy-Villacoublay, France
[d] Institut Curie, Flow Cytometry Department, F-75006, Paris, France
[e] National Cytometry Platform, Department of Infection and Immunity, Luxembourg Institute of Health, Luxembourg
[f] Service D'Hématologie et Laboratoire de Recherches Biochirugicales (Fondation Carpentier), AH-HP, Georges Pompidou European Hospital, F-75015, Paris, France
[g] Laboratory of Biological Structure Mechanics (LaBS), Department of Chemistry, Materials and Chemical Engineering "Giulio Natta", Politecnico di Milano, Milan, Italy
[h] PNAS, Institut Galien de Paris-Sud, Faculté de Pharmacie, Université Paris-Sud, CNRS UMR8612, 5 Rue JB Clément, Chatenay Malabry, France
[i] Service Chirurgie Cardique et Laboratoire de Recherches Biochirugicales (Fondation Carpentier), AH-HP, Georges Pompidou European Hospital, F-75015, Paris, France

ARTICLE INFO

Keywords:
Biomedical engineering
Bioengineering
Biophysics
Cardiology
Haematology
Total artificial heart
Bioprosthetic
Carmat
Hemocompatibility

ABSTRACT

The Carmat bioprosthetic total artificial heart (C-TAH) is a biventricular pump developed to minimize drawbacks of current mechanical assist devices and improve quality of life during support. This study aims to evaluate the safety of the hybrid membrane, which plays a pivotal role in this artificial heart. We investigated in particular its blood-contacting surface layer of bovine pericardial tissue, in terms of mechanical aging, risks of calcification, and impact of the hemodynamics shear stress inside the ventricles on blood components. Hybrid membranes were aged in a custom-designed endurance bench. Mechanical, physical and chemical properties were not significantly modified from 9 months up to 4 years of aging using a simulating process. Exploration of erosion areas did not show no risk of oil diffusion through the membrane. Blood contacting materials in the ventricular cavities were subcutaneously implanted in Wistar rats for 30 days as a model for calcification and demonstrated that the in-house anti-calcification pretreatment with Formaldehyde-Ethanol-Tween 80 was able to significantly reduce the calcium concentration from 132 μg/mg to 4.42 μg/mg ($p < 0.001$). Hemodynamic simulations with a computational model were used to reproduce shear stress in left and right ventricles and no significant stress was able to trigger hemolysis, platelet activation nor degradation of the von Willebrand factor multimers. Moreover, explanted hybrid membranes from patients included in the feasibility clinical study were analyzed confirming preclinical results with the absence of significant membrane calcification. At last, blood plasma bank analysis from the four patients implanted with C-TAH during the feasibility study showed no residual glutaraldehyde increase in plasma and confirmed hemodynamic simulation-based results with the absence of hemolysis and platelet activation associated with normal levels of plasma free hemoglobin and platelet microparticles after C-TAH implantation. These results on mechanical aging, calcification model and hemodynamic simulations predicted the safety of the hybrid membrane used in the C-TAH, and were confirmed in the feasibility study.

1. Introduction

Heart transplantation offers the most effective therapy for patients with end-stage heart failure but is severely limited by organ shortages and, in some cases, by patient comorbidities [1]. The use of mechanical circulatory support, and in particular left ventricular assist devices (LVAD), has been shown to offer a valuable therapy for these patients but only indicate for mono-ventricular heart disease compared to an optimal

* Corresponding author.
E-mail address: david.smadja@aphp.fr (D.M. Smadja).

https://doi.org/10.1016/j.heliyon.2019.e02914
Received 19 July 2019; Received in revised form 12 November 2019; Accepted 21 November 2019

medical management [2]. Nowadays, 2,500 patients are implanted annually in the USA with mechanical circulatory devices and the INTERMACS registry database includes over 20,000 patients [3]. The Carmat Total Artificial Heart (C-TAH) was developed as a heart replacement device in new Physiological Heart Replacement Therapy for patients at risk of imminent death from bi-ventricular failure. It is an implantable, electro-hydraulically actuated and, pulsatile biventricular pump support [4], designed to promote quality of life, minimize thromboembolism events and bleeding that are common complications of continuous-flow LVAD. The C-TAH comprises a left and right ventricle, each with a blood compartment and a hydraulic fluid (drive-unit), separated by a hybrid membrane made of two layers glued together. One layer, in contact with the hydraulic fluid, is made of polyurethane (PU), the other which is in contact with the blood, is made from bovine pericardial tissue, chemically treated with glutaraldehyde to provide long-term tolerance and hemocompatibility [5, 6]. The concept of xenogeneic pericardial tissue treated with glutaraldehyde has already been used in bioprosthetic heart valves for more than 40 years after two successful clinical trials in the 70s and the 80s [7,8] and represented more than 80% of the 200,000 heart valve replacements performed worldwide in 2006 [9].

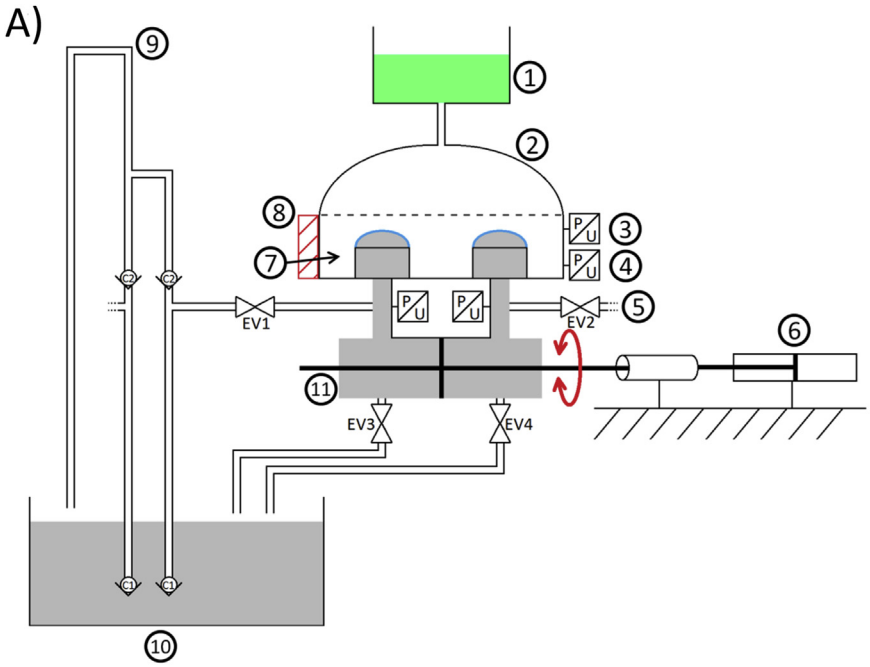

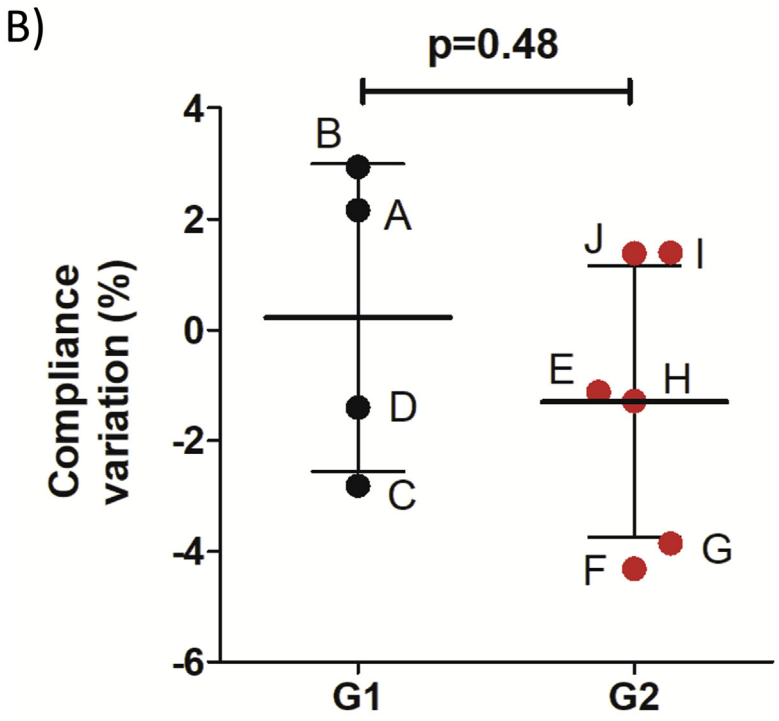

Figure 1. Endurance bench and measures of compliance. A: Schematic view of the endurance bench used for membranes aging test, description of the different components of the bench test used for validation of membrane resistance: 1) PBS Kathon reservoir; 2) Glass dome; 3) Pressure sensor; 4) Pressure sensor; 5) Pressure sensor; 6) Hydraulic pump; 7) Bench test chamber filled by PBS with Kathon; 8) Metallic tank; 9) Silicon oil supply; 10) Silicon oil reservoir; 11) Hydraulic actuator filled with silicon oil; *) C-TAH hybrid membranes.B: Kinetic of volume-loss to evaluate the variation of the membrane compliance after endurance test in percentage. Group 1 is the low number of cycles aging group (black) with membranes A, B, C and D; Group 2 is the high number of cycles aging group (red) with membranes E, F, G, H, I and J.

The hybrid membrane separating the ventricle and the drive-unit is a highly critical device component; as the rupture or degradation of this membrane would lead to an instant loss of pump performance and significant risk of death for the patient. Hence, the chemical and mechanical stability of the hybrid membrane after aging are important parameters to investigate. General requirements for *in vitro* durability testing of blood pumps are given by the ISO 14708–5 [10] and the recommendations by of the National Clinical Trial Initiative Subcommittee (NCTIS recommendations) [11]. Thus, NCTIS recommends accelerated durability tests of either the complete system or single component with accelerated aging mechanical tests. Hemodynamic patterns are expected to influence also hemocompatibility and safety of C-TAH because of potential blood damages related to shear including induced hemolysis [12, 13], platelets activation [14] and vWF degradation [15] triggering acquired von Willebrand syndrome (AVWS) [16]. Thus, preclinical evaluation of the hemodynamic shear stress by using a robust numerical methodology is essential to predict the hemocompatibility performance and to optimize the ventricular design. For this purpose, Computational Fluid-dynamics (CFD) and Fluid-Structure Interaction (FSI) models can be employed to investigate the kinematics of the C-TAH components, e.g. the membrane and the leaflets, and predict the potential damage on blood elements.

This study explores the safety of the hybrid membrane used in the C-TAH with a particular emphasis on mechanical aging and calcification model. We used hemodynamic simulations to compare the blood handling characteristics of this device, i.e. hemolysis, platelet activation and AVWS. We aimed at verifying the absence of hybrid membrane calcification, glutaraldehyde toxicity and confirming the hemodynamic safety on patient hemostasis with clinical feasibility study [4].

2. Material and methods

2.1. Endurance bench

A novel custom-designed endurance bench was used by Carmat to perform the mechanical endurance test of the hybrid membrane of the C-TAH (Figure 1A). The mechanical resistance through time of the membranes and the impact of the aging on their properties were tested with this appropriated bench test. The hydraulic test pressure was generated with a blood-simulating fluid: phosphate buffered saline (PBS) with Kathon at 5 cP viscosity and an actuating fluid using silicone oil with a 20 cP viscosity to mimic hydraulic actuation contacting surfaces of the C-TAH in vivo. The fluid movement of the bench had a frequency of 10Hz with a 30 ml moved volume to perform accelerated aging. The flow rate was 4 l/min and the system maintained at 37 °C.

2.2. Tested membranes

Hybrid membranes made of PU and bovine pericardium, identical to those used in clinical trials, were tested. The dimensions of the membranes are 80 mm × 100 mm with an ovoid form, the thickness is 700μm: the hybrid membrane is made of one layer of PU Chronoflex ARLT© (thickness = 350μm) and bovine pericardium from Neovasc Inc. (Vancouver, Canada) (thickness = 350μm).

2.3. Endurance test

Ten hybrid membranes, labeled from A to J were tested on the endurance bench, with five different numbers of cycles (Table 1). For each number of cycles, two membranes were tested. These amounts of cycles were separated in two groups: low amounts values corresponding to aging group 1, high amounts values corresponding to aging group 2. For each of the ten aged membranes, after the end of the test on the endurance bench, the pericardium layer was removed and samples of PU were trimmed after the end of the test on the endurance bench.

Table 1. Membrane tested in endurance bench.

Aging group	Membrane	Number of cycles	Duration of the test	In vivo equivalent
1	A	3.61×10^7	64 days	9 month
	B	3.61×10^7	64 days	9 month
	C	8.73×10^7	111 days	22 month
	D	8.73×10^7	111 days	22 month
2	E	1.11×10^8	124 days	28 month
	F	1.11×10^8	124 days	28 month
	G	1.49×10^8	192 days	38 month
	H	1.49×10^8	192 days	38 month
	I	1.85×10^8	236 days	4 years
	J	1.85×10^8	236 days	4 years

2.4. Compliance

The membrane compliance is the deployment resistance of the membrane, measured by the moved volume depending on the applied pressure; it was determined with kinetic of volume-loss at the same pressure during the endurance test on the endurance bench.

2.5. Mechanical degradation – differential scanning calorimetry

Differential Scanning Calorimetry (DSC) is often used to characterize polymer structure; the glass transition temperature measured is correlated indeed with the state of the polymer. Change in its state or degradation of the polymer causes a modification of the glass transition temperature.

DSC was performed on four different samples of each of the ten membranes. The test was run in accordance with the ISO norm standard [17], in order to explore the degradation of the material. Analysis was performed on with a DSC Q2000 (TA Instruments, Newt Castle, Delaware, USA), in standard mode with airtight aluminum sample holders. The purge gas used was quality nitrogen with a flow rate of 50 ml/min flow rate. Temperatures ramps and times for the analysis were: isotherm at -90 °C for 5min, from -90 °C to 200 °C with a 10 °C/min gradient, isotherm at 200 °C for 5min, from 200 °C to -90 °C with a 10 °C/min gradient, isotherm at -90 °C for 5min then from -90 °C to 200 °C with a 10 °C/min.

2.6. Fourier-Transform Infrared Spectroscopy Spectroscopy

Fourier-Transform Infrared Spectroscopy Spectroscopy (FTIR) is used to characterize polymer integrity; a specific spectrum is obtained due to the absorption of the different chemical functions. The chemical degradation of the polymer triggers a shift in the peaks of the spectrum or decrease in band intensities. To analyze the PU membrane, we compared the spectra obtained for the ten tested membranes to one obtained from a not aged control membrane. The analyses were performed on an IRAffinity-1 Spectrometer (Shimadzu, Kyoto, Japan) with an ATR Base (MIRacle PIKE Technologies). Characteristic functions and corresponding infrared bands of the PU were chosen and monitored: –NH absorbing at $3321cm^{-1}$ (1), two –CH2 at $2937cm^{-1}$ (2) and $2862cm^{-1}$ (3) of the carbon chain, –C=O at $1739cm^{-1}$ (4), C=C of the aromatic at $1592cm^{-1}$ (5), C–C of the aromatic at $1403cm^{-1}$ (6), C–O–C of the carbonate function C–O–C=O at $1251cm^{-1}$(7), C–O at $1110cm^{-1}$ (8), C–O–C of the urethane function C–O–C=O at $1068cm^{-1}$ (9). FTIR was performed on four samples of PU for each aged membrane and one non-aged control membrane; ten scans were recorded for each sample.

2.7. Surface characterization

2.7.1. Electronic microscopy

We performed electronic microscopy to explore the PU surface of the aged membranes in order to highlight possible erosion areas or weak

points. The microscope used was a S260 Scanning Electron Microscope (Cambridge Scientific Corp, Watertown, Massachusetts, USA). The samples were fixed in 2.5% glutaraldehyde with 0.1M Phosphate Buffer pH 7.4 overnight. Then, washed in PB – 3 × 15min and fixed in Osmium solution (1% OsO_4, 0.1M PB) for 1h at 4 °C before getting washed in 0.1M PB solution for 15min two times, and H_2O solution for 5min. For dehydration, the solutions used were 30% Ethanol (EtOH) for 15min, 50% EtOH for 15min, 70% EtOH for 15min, 95% EtOH for 15min, 100% EtOH two times for 20min, Hexamethyldisilazane (HMDS)/EtOH at ratio 1/1 for 10 min, 100% HMDS for 10min then dried overnight. The next day samples were glued on pads with metallic glue, then left for 24 h before metallization and observation.

2.7.2. Surface topography

Membranes D, E and F were tested, using a non-contact surface topography system: Altisurf 500 (Altimet, Sainte-Hélène-du-Lac, France). For each membrane, four samples were analyzed, and three profiles for each sample were measured. Sensor size used was 300 μm, with mono-directional measure mode. The resolution was 1μm in X and 5μm in Y, with an acquisition frequency of 100Hz and a measurement speed of 100 μm/s for the contact zone, and for the working zone a 30Hz acquisition frequency with a measurement speed of 30 μm s^{-1}. The tests were performed in compliance with the ISO norm standard [18].

2.8. Raman spectroscopy

Raman spectrometry was used to detect the presence of oil diffusing inside the PU membrane. This analysis technique highlights the composition of a polymer; a specific Raman shift is observed if other chemical species appear inside the polymer. Four membranes: E, F, G and H of advanced aging have were tested. For each tested membrane, both faces of two samples were investigated. The analysis was performed with a Xplora microspectrometer from HORIBA Scientific, coupled to a high-performance Raman analysis module. The excitation wavelength was 785nm, with characteristic bands at 492cm^{-1} for Silicon oil and 1618cm^{-1} for the PU. The samples were analyzed on a Z profile on constant XY point, the Z profile acquisition size was between -20μm and +80μm inside the sample, with a pace of 5μm and time acquisition of 10s for each point.

2.9. Gas Chromatography with Mass Spectrometry

Gas chromatography coupled with Mass Spectrometry (GCMS) was used to detect the presence of silicon oil in the aging solution of Kathon-PBS for all the endurance tests performed. This technique can highlight the presence of chemical residues even at very low concentrations. All analyses were performed on a GCMS QP2010 from Shimadzu (Kyoto, Japan), using a DB-5ms column, (length 30m, thickness 0.25μm, and diameter 0.25mm). The temperature gradient used for the membranes A and B was: from 40 °C to 280 °C (10 °C/min) then 280 °C for 5min. The final step was increased to 8min for the other membranes (C– I). For quantitative analyses, a splitless injection was performed at 250 °C with 1μl for the membranes A and B and then 0.5μl for the others. A scan mode was employed for qualitative analyses.

2.10. In-vivo calcification assay

The study was designed in accordance with the ISO norms [19, 20]. The *in vivo* tests were performed to study the calcification potential of the components of the ventricular cavity in of the C-TAH. The calcification model chosen was subcutaneous implantation in rats of round pieces of bovine pericardium tissue and expended Polytetrafluoroethylene (ePTFE). The positive control chosen was bovine pericardium fixed with glutaraldehyde and not treated with an anti-calcification treatment. The two tested materials were bovine pericardium with dedicated in-house anti-calcification treatment FET (Formaldehyde-EtOH-Tween 80) [21] and ePTFE (top of C-TAH ventricle cavity in contact to blood). The three types of materials were tested; for each type of material 40 samples were implanted subcutaneously into 30 Wistar Rats (male and female).

Four samples of pericardium were implanted per rat, with different random combinations randomly assigned using the computer random number generator with Excel 2000. The implantation duration was 30days in 12days old rats at the implantation. The test items were pieces of 8mm diameter and 0.8mm thickness. For the implantation procedure, animals were anesthetized with a mixture of 3% isoflurane (VETFLURANE, Virbac) and compressed air. The skin was cleaned with 70% ethanol and povidone iodine solution. Buprenorphine (BUPRECARE, Animalcare Limited) 0.02 mg/kg by subcutaneous route and 2.5% enrofloxacin (BAYTRIL, Bayer) 10 mg/kg by subcutaneous route were administered before membrane implantation. The volume to be administered was calculated according to the bodyweight recorded on Day 0. Before implantation, membranes were successively rinsed in 3 different and successive baths of sterile 0.9% NaCl solution (COOPER). On Day 30, animals were anesthetized with a mixture of 3% isoflurane and compressed air, sacrificed by cervical dislocation, and the membranes were explanted. For the groups of pericardium tissues samples, membranes were transferred in an individual weighted Teflon tube. The tubes were put in a drying chamber under vacuum at 50 °C for during 3hours and 10min. After cooling, the tubes containing the dry membranes were weighted in order to determine the individual membrane weight. For the group of ePTFE samples, the membranes were transferred in an individual weighted glass tube. The tubes were put in a drying chamber vacuum at 50 °C for during 3hours and 15min. After cooling, the tubes containing the dry membrane were weighted in order to determine the individual membrane weight. A calcination of these membranes was performed by placing the glass tubes into an oven at 600 °C for 9hours. The whole samples were dissolved with 2ml of HNO_3 in 7ml Teflon vials on hot plates for 24hours at 90 °C, then diluted with ultrapure water (resistivity = 18.2MΩ) in 100ml and 30ml precleaned (0.1N HCl) polycarbonate vials, with internal standard (In–Re) added as solution (0.3g for 30ml of final solution) leading to concentration close to 5ppb. The diluted samples then assayed for Calcium determination with inductively coupled plasma mass spectrometry (ICP-MS) using ICP-MS (Instrument: Serie X 2 from Thermo Electron) and calibrated using a calibration curve with five standard solutions.

2.11. Hemodynamic simulations

The hemocompatibility of the device is also linked to its hemodynamics. Indeed, it is important to have a reliable blood flow description to assess the blood damages induced by the implanted bioprosthesis. The important parameters to calculate are the shear forces endured by the blood inside the blood volume during the contraction cycle and the wall shear stresses during the contraction cycle. Numerical simulations are a good way to extract these data. Our numerical model includes both ventricles of the C-TAH with the oil and blood parts, the membrane and the valves. In order to simulate the interactions between fluids and solids, an FSI model coupled with CFD simulations was developed [22, 23]. The FSI simulation well describes the displacement and the stress of the solid parts. However, it fails to accurately describe the fluid, especially for derivative parameters like the wall shear stresses. Nevertheless, the macroscopic fluid flow is reliable, if the movements of the solid parts are well captured. CFD simulations were subsequently used to have an accurate fluid description of the blood behavior inside the ventricular chamber [11]. The displacements of the membranes and valves were extracted from the FSI simulation and used to define as moving boundary conditions in the CFD simulations. Indeed, CFD simulations allow the implementation of moving walls as boundary conditions of the fluid domain, i.e. for valves and membranes. The hemodynamic boundary conditions, in terms of pressure curves and flow rate, were identical in FSI and CFD simulations. Coupling the FSI and the CFD simulations yielded the displacement of the solid parts (FSI) and an accurate blood

flow description (CFD). Briefly, the geometrical model was built from the Computer Conception Aided Design model of the C-TAH, except for the valves, which are were simplified with only three leaflets by discarding the stent frame. The boundary condition prescribed at the oil inlet was a flow rate corresponding to a nominal case at of 5.4 l/min (heart rate = 90bpm, stroke volume = 60ml). The systolic time was one third of the cycle time. A nominal pressure of 120mmHg was set at the aortic outlet against 35 mmHg at the pulmonary outlet. The mitral and the tricuspid pressures were set to 0mmHg as a reference pressure. The results of the simulation provided data consistent with the observations.

These simulations, and some technicalities of the FSI settings, are described more in depth in a previous papers of ours [22]. Simulations produced as outputs the numerical values of the forces endured by the bloodstream, inside the C-TAH during the cycles of contraction. These forces, need to be linked to the induced hemolysis [12, 13], platelets activation [14] and vWF degradation [15]. Hemolysis has been previously studied especially with regard to Ventricular Assist Devices (VAD), because of the continuous exposition of the red cells to a high shear rate in those devices due to the rotary pump used [24]. In our case, the pump is pulsatile, with very short time of exposure to high shear stresses. The threshold commonly used in studies of VAD for hemolysis is usually set to 150Pa [25]. However, in order to have a more accurate estimation of the impact of the device on the red blood cells, we used the following index of hemolysis equation, taking into account both the shear stress (τ in Pa) and the exposure time (t in second) [26] with the index of hemolysis: $\boldsymbol{IH}(\%) = 3.458 \times 10^{-6} \times \boldsymbol{\tau}^{2.0639} \times \boldsymbol{t}^{0.2777}$. Thus, it is possible to have a precise estimation of the maximum hemolysis induced by the C-TAH contraction cycle. The platelets activation threshold normally used is 50Pa [25]; however, a recent study proposed a formula connecting the shear stress and the exposure time for a more accurate estimation of platelets activation [27]; the platelets activation index was calculated as follows: $\boldsymbol{PA}(\%) = 4.08 \times 10^{-3} \times \boldsymbol{\tau}^{1.56} \times \boldsymbol{t}^{0.8}$. We also chose to use for our simulations the threshold of 17.5Pa for the high molocular weight multimers (HMWM) of vWF degradation in our simulation [28, 29]. Hemolysis and platelets activation are different from vWF degradation because of the plasticity of the membranes. Very high shear stress for short duration can be less problematic than a mild shear stress occurring for a long time.

2.12. Clinical feasibility study of Carmat Total Artificial Heart implantation

This was a single-arm, prospective, non-blinded and non-randomized study of 4 patients conducted in 4 four French centers. The study was approved by the French National Agency for Medicines and Health Products Safety, and the Paris' Regional Ethics Committee. The study was registered in the European Databank on Medical Devices (CIV-FR-13-09-011615). Plasma from Heartmate II patients were sampled according to register number 1922081. All patients had signed the informed consent, and the study was performed in accordance with the Declaration of Helsinki [30].

2.12.1. X-Ray Microtomography in C-TAH explanted patient

X-Ray Microtomography on explanted membranes from the clinical trial was performed using the CERN (European Organization for Nuclear Research). The X-ray source was an ESRF, ID19, with energy of 115keV. The number of projections was 6000, with a pose time of 0.03s, and a voxel size of 12.9 μm^3. Acquisitions were made at room temperature and room pressure, in the conservation solution (1X PBS, 0.6% Glutaraldehyde).

2.12.2. Laboratory assessment

Blood samples were drawn pre-operatively and weekly thereafter. All samples were collected on 0.129 M trisodium citrated tubes (9NC BD Vacutainer, Plymouth, UK). Laboratory assessments were done on platelet poor plasma (PPP) obtained after centrifugation twice at 2500g for 15min. PPP was frozen and stored at -80 °C until analysis.

2.12.3. Quantification of residual glutaraldehyde, plasma free hemoglobin and platelet microvesicles in plasma before and after C-TAH implantation

Blood samples were drawn pre-operatively, during surgery, daily during the ICU period and weekly thereafter. All samples were collected on sodium heparin for plasma free hemoglobin and 0.129M trisodium citrate tubes (9NC BD Vacutainer, Plymouth, UK) for other analyses. 10µl of Acetone-D_6 was added to 200µl of citrated plasma and loaded on a Phree tube to remove proteins and phospholipids from plasma samples without negatively affecting the recovery of our target analyte glutaraldehyde. After adding 800µl of acetonitrile and a 1% formic acid and, a 5min centrifugation was performed, the organic layer was withdrawn, and the pellet reconstituted in 20µL of 5.4M HCl and 500µl of 2,4-dinitrophénylhydrazine (DNPH; 2 g/l in acetonitrile) before Liquid Chromatography-Mass Spectrometry (LC-MS/MS) injection. The analytical method was adapted from Menet et al [31]. The calibration curve was made by adding glutaraldehyde in plasma until the value of 5 µg/mL ($r^2 = 0.9737873$). The limit of detection of glutaraldehyde was estimated at 0.01 µg/ml.

Plasma free hemoglobin concentrations were calculated using a Lambda 25 EV/VIS Spectrometer (Perkin Elmer Instruments, Waltham, Massachusetts, United States) with second derivative spectrophotometry at specific wavelengths between 576nm and 561 nm. For microvesibles (MV) quantification, thawed plasma samples were 1/10 diluted in physiological serum and stained with anti-human fluorochrome-coupled antibodies for MV phenotyping: Annexin V Pacific Blue (ebioscience) and CD41 Fluorescein isothiocyanate FITC (FITC, Beckman Coulter). Fluorescent calibrated beads Megamix-Plus SSC (Biocytex) were used to define MV size based on side scatter parameter according to manufacturer instructions. MV concentrations were assessed by addition of an internal calibrator, AccuCount fluorescent particles (Shperotech) with a known concentration of particles per volume. Acquisitions of stained MV and calibrated beads were performed with a LSR Fortessa SORP cytometer (Becton Dickinson). Analyses were done with FlowJo 10 software (TreeStar).

2.13. Statistical analysis

Data were analyzed using the non-parametric Mann-Whitney test. Therefore data are shown as median [Q1; Q3]. All statistical analyses were performed with GraphPad Prism 5 software (GraphPad Software Inc., San Diego, CA, United States) and StatView software package (SAS, Cary, NC, USA). Differences were considered significant at $p < 0.05$.

3. Results

3.1. Mechanical aging did not induce hybrid membrane degradation

Membrane compliance, measured continuously during the aging test on the endurance bench as the kinetic of volume-loss under the same pressure, remained unchanged between the two groups (0.375 [-2.47; 2.75] vs -1.21 [-3.98; 1.38]; p = 0.476, Figure 1B). No compliance variation superior to 5% in any of the investigated membranes was recorded. The polymeric state of the PU evaluated by the measurement of glass transition temperatures in by differential scanning calorimetry (DSC) did not show any significant differences between the two groups (-28.7 [-29.2; -27.33] vs -28.2 [-29.1; -27.4]; p = 0.83, Figure 2A).

The potential risks of polymer hydrolysis and interaction with oil were investigated by Fourier-Transform Infrared Spectroscopy. The aromatic and carbon chains of the polymer as well as functions containing oxygen atoms were mostly analyzed. Here are presented one spectra for each time of aging (Figure 2B). Intensities of the investigated bands exhibit only slight variations. These observed differences remained

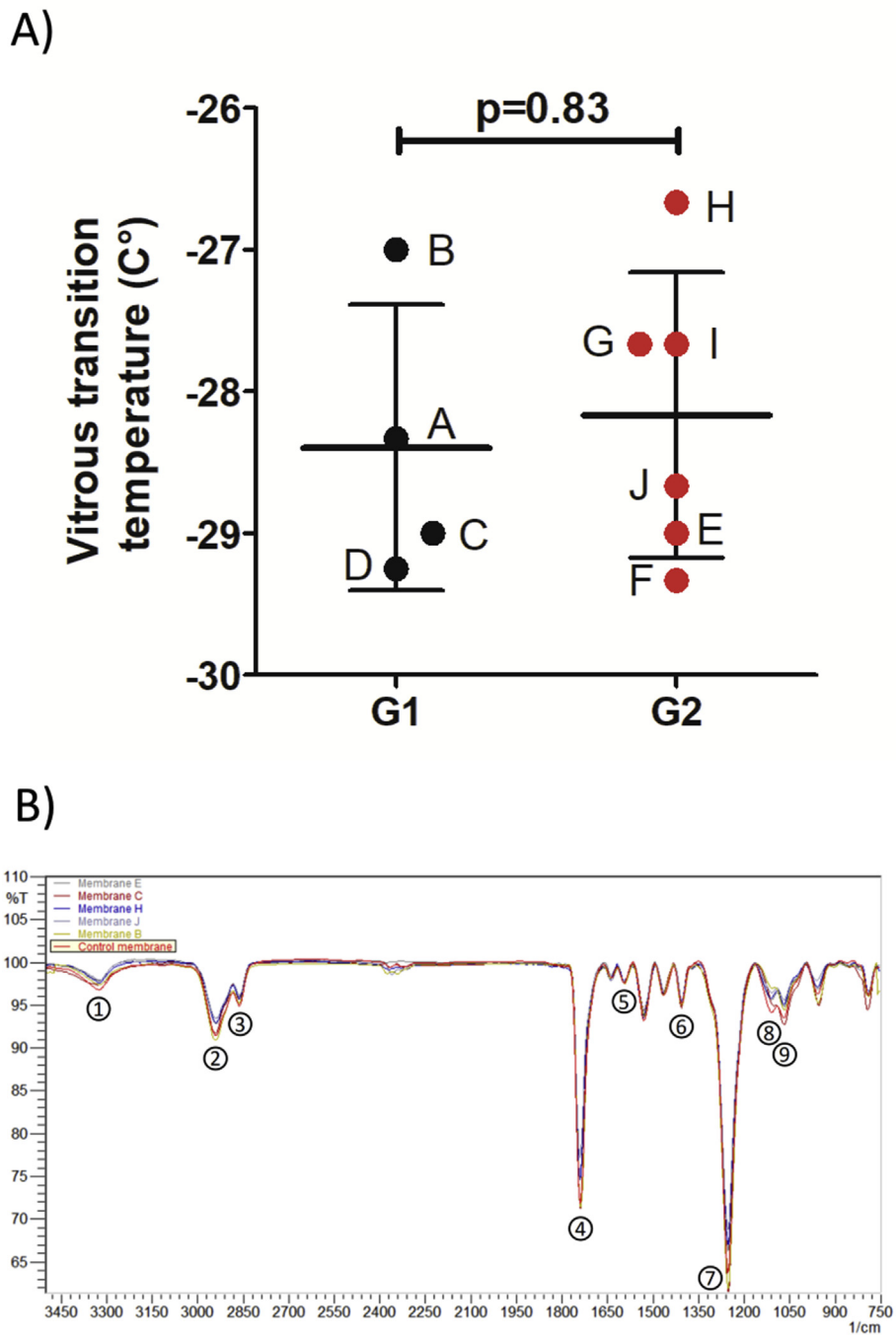

Figure 2. Physical tests to evaluate the aging of the membranes. A: Measures of the glass transition temperatures obtained by Differential Scanning Calorimeter for the membranes, separated in Group 1: low number of cycles aging group (black) with membranes A, B, C and D; and Group 2: high number of cycles aging group (red) with membranes E, F, G, H, I and J. B: Infrared Absorption Spectra of one membrane for each of the 5 amount of cycles (membranes B, C, E, H, and J) and the non-aged control membrane; peaks are corresponding to-NH absorbing at 3321 cm^{-1} (1), two –CH2 at 2937 cm^{-1} (2) and 2862 cm^{-1} (3) of the carbon chain, –C=O at 1739 cm^{-1} (4),C=C of the aromatic at 1592 cm^{-1} (5), C–C of the aromatic at 1403 cm^{-1} (6), C–O–C of the carbonate function C–O–C=O at 1251 cm^{-1}(7), C–O at 1110 cm^{-1} (8), C–O–C of the urethane function C–O–C=O at 1068 cm^{-1} (8).

constant and consistent for a given sample. More importantly, no band shift was observed between the control and all the aged membranes in the transmission spectra indicating that the chemical groups were not modified and the functions remained stable over time.

3.1.1. Surface characterization

The observations made by scanning electronic microscopy of the PU surface brought to light two different areas of potential erosion on the face in contact with oil (Figure 3A). The two erosion areas were found in all the aged membranes, and showed signs of superficial deterioration. Thus, we considered these areas as a potential location of breach with the risk of silicon oil diffusion through the PU and oil leaking into the blood compartment. The erosion areas are located in the contact zone and the working zone (Figure 3B).

3.1.2. Surface topography

Surface Topography was used to explore the importance of these erosions and their depth in the three membranes showed no risk of potential break through (Figure 3C). The maximum depth observed was 16.2μm, the thickness of the PU membrane being 350μm, and thus this represented less than 5% of the thickness of the PU membrane. The mean depth of the erosions for the membranes for the contact zone was 15.1μm (min = 13.7μm, max = 16.2μm) for D membrane, 10.5μm (min = 3.9μm, max = 14.8μm) for E membrane and 8.0μm (min = 3.9μm, max = 12.6μm) for F membrane. The erosions are more important on the contact zone than on the working zone where the mean depth was 5.5μm (min = 4.96μm, max = 6.35μm) for D membrane, 9.7μm (min = 2.8μm, max = 13.9μm) for E membrane and 3μm (min<2μm, max = 9μm) for F membrane.

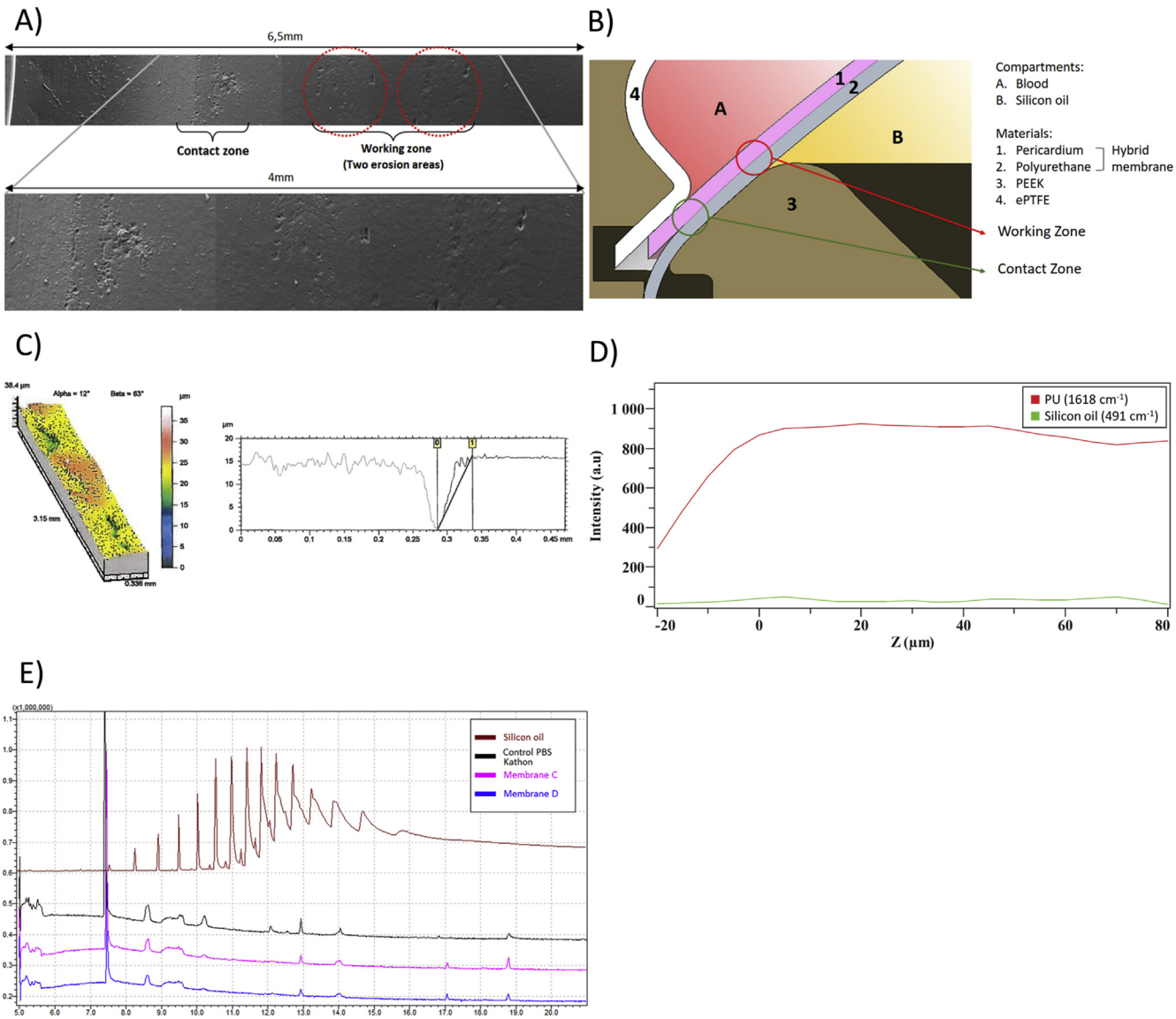

Figure 3. Surface exploration and permeability. A: Reconstruction using Electronic Microscopic images investigating the two erosion zones on the PU membrane: contact zone on the left corresponding to the zone in contact with the PEEK, and working zone on the right in contact with the oil. B: Cross sectional view of a schematic representation of the disposition of the hybrid membrane inside the C-TAH, with the two erosion areas: the working zone and the contact zone. C: Topographic mapping of the surface of one erosion area on the left, with the topographic profile acquired during exploration of the erosion on the right. D: Raman spectroscopy one membrane, PU wavelengh = 1618 cm^{-1}; silicon oil wavelengh = 491 cm^{-1}, Z profile assessing the absence of silicon oil inside the PU membrane. E: Gas Chromatography coupled with Mass Spectrometry performed on the aging solution of PBS-Kathon used in the endurance bench. Brown: positive control of silicon oil; Black: negative control of non-aged PBS-Kathon; Purple: PBS-Kathon used for the aging of the membrane C; Blue: PBS-Kathon used for the aging of the membrane D.

3.1.3. Raman spectrometry

Raman spectrometry enabled us to explore potential presence of diffusing oil inside the membrane (Figure 3D). The intensity of silicon oil band measured at different Z values was found not different from the background noise. The signal of the PU is increasing before the laser focus point entered the material because of light diverging from this point of focus, generating Raman signal of the PU and detected. Therefore, we concluded that no trace of silicon oil was present inside the membranes tested, this result was observed for two different aging times.

3.1.4. Gas Chromatography with mass spectrometry

Finally, Gas Chromatography coupled with Mass Spectrometry (GCMS) attested the absence of silicon oil in the aging solution PBS-Kathon (Figure 3E) for every tested membrane. The peaks of the control PBS-Kathon were strictly identical to those of the aged PBS-Kathon, no additional chemical species were detected in these solutions, and no profile similar to the positive control of silicon oil was seen. The results of these tests showed that mechanical aging does not alter the ability of the membrane to prevent oil diffusion to the blood cavity.

3.2. Pretreatment of membrane significantly decreases calcification in rats

Calcium quantification in the different materials subcutaneously implanted in rats showed after explantation (Figure 4A) a strong effect of the anti-calcification treatment (Figure 4B). The positive control was the pericardium without treatment, with high Calcium concentrations (132 ± 24.7 µg/mg), significantly higher to the Pericardium with anti-calcification treatment (FET) (132 [110; 148] vs 0.997 [0.897; 2.5]; $p < 0.0001$) and to the ePTFE (132 [110; 148] vs 23.7 [12.4; 31.6]; $p < 0.0001$). Thus, anti-calcification treatment was effective on the

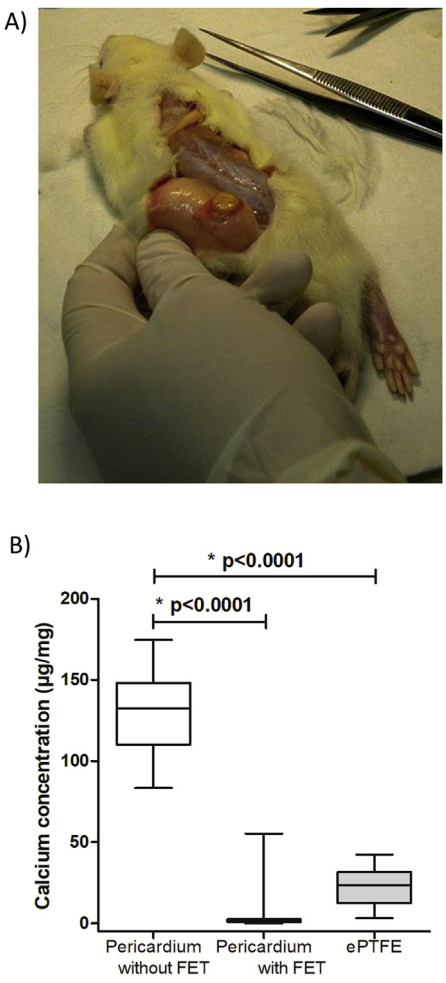

Figure 4. *In-vivo* calcification test. A: Picture of subcutaneous membrane explant on a Wistar rat after euthanasia. B: Diagram of the calcium concentration (in µg/mg) in the different membranes: pericardium without anti-calcification treatment as positive control, Pericardium with anti-calcification (FET) treatment and ePTFE.

pericardium and the material used in the blood cavity of the C-TAH did not trigger important calcification reaction in this rat model.

3.3. Hemodynamic simulation confirms safety regarding red blood cells, platelets and von Willebrand factor

The FSI simulations implemented in the CFD enabled us to extract graphs (Figure 5), showing for both ventricles the distribution histograms of the shear forces (Figure 5A) and the cumulative curves of shear stress repartition (Figure 5B) presenting the minimum, mean and maximum blood volume concerned for each shear value. More than 90% of the blood volume endured shear stresses inferior to 1 Pa during one cycle of contraction, less than 0.03% shear stresses above 17.5 Pa, less than 0.001% shear stresses above 50 Pa and nothing above 150 Pa. Since the values over 17.5 Pa are inferior to 0.03% of the volume for both ventricles the simulation predicted no vWF degradation.

In order to better evaluate the risk of hemolysis and platelets activation we used the cumulative shear stress curves (Figure 5C and D). To estimate the average impact of the contraction cycle on hemolysis and platelets activation using the equations related to HI and PA. We used the mean shear value endured by the blood volume during one cycle of contraction (700ms) of 0.23 Pa in the left and right ventricle for an entire contraction cycle (Table 2). The mean hemolysis index was inferior to 1.51×10^{-7}%, lower than an estimated physiological value since the estimated hemolysis index after one passage through the blood system was is 5.8×10^{-4}% [32]. The platelets activation index was 3.1×10^{-4}% for both ventricles.

We also explored the critical conditions, the areas with a shear stress above 17.5 Pa were visible with red dots during the cycle on the hemodynamic simulation (Supplementary video 1 and 2), and the graph below the simulation shows the blood volume percentage enduring this shear stress. We determined that a peak of shear existed at the ejection valve during systole between 450ms and 650ms for 200ms. During the ejection phase, the blood flow reached a high speed so the blood volumes exposed at this high shear stress were exposed for a very short duration. In order to estimate the impact of this peak, we used the max value in the mean cumulated curve for the highest 1% of blood volume on the time of the peak during systole. At 3.71Pa in the left ventricle, 3.75Pa in the right ventricle for 200ms (Table 2), the hemolysis index was inferior to 3.4×10^{-5}% for both ventricles, while platelet activation index determined was 8.85×10^{-4}% for right ventricle and inferior to 8.70×10^{-4}% for left ventricle. These simulations were in favor of a very low percentage of hemolysis and platelet activation with C-TAH.

4. Confirmation of hybrid membrane safety in feasibility study of C-TAH implantation in 4 patients

We first wanted to confirm absence of calcification in C-TAH implanted patients. We thus performed X-Ray microtomography analysis of the hybrid membrane after explantation [30]. In Figure 6A, we showed the 3D model of the hybrid membrane with six acquired plan from X-Ray microtomography located on this membrane. No calcification on both left and right membrane was detected on the areas in contact with blood, (Figure 6A, patient number 3, after 9 month of implantation). Only area at the extremity of the membranes presented calcification, not in contact with blood and not in a mechanically moving area, after the sealing ring and the contact zone, - this area is a dead end between the two solid parts in polyetheretherketone (PEEK) (see Figure 3B).

Moreover, we wanted to ensure the absence of residual glutaraldehyde after C-TAH implantation. Plasmatic glutaraldehyde quantification before and after C-TAH implantation was performed (Figure 6B) and showed no noticeable increase after implant for the three patients, with values close or equals to the detection limit.

Finally, we confirmed the *in-silico* simulation results on blood damage in patients implanted with C-TAH, by quantification of hemolysis with plasma free hemoglobin and platelet activation with quantification of platelet MV during follow-up. As proposed in Figure 6C, no significant hemolysis was been found in the three patients implanted with C-TAH, since median levels were between 5 to 10 times lower than the pathological cutoff defined by Intermacs for Mechanical Circulatory Support [33]. For platelets activation, no significant increase was noticed (Figure 6D), contrarily to the HeartMate II (HM2, (5 patients between 1 and 6 months of implantation). All patients with C-TAH and HM2 had long-term antiplatelet therapy with aspirin.

5. Discussion

The prospect of successful mechanical circulatory assistance as a heart replacement device, in patients at risk of imminent death from biventricular failure in destination therapy, depends upon the device its ability to obtain good quality of life secondary to good hemocompatibility in contrast to mechanical circulatory support currently existing. Also good durability in terms of mechanical resistance and potential deterioration of the hybrid membrane is required. The applied technique to make hybrid membranes with bovine pericardial tissue and PU in the C-TAH has shown to be efficient in terms of preclinical evaluation of hemocompatibility [5, 34, 35] and clinical feasibility in the four first implanted patients with a maximal duration of nine months for patient number 2 [4,30,36]. The purpose of the present study was to evaluate

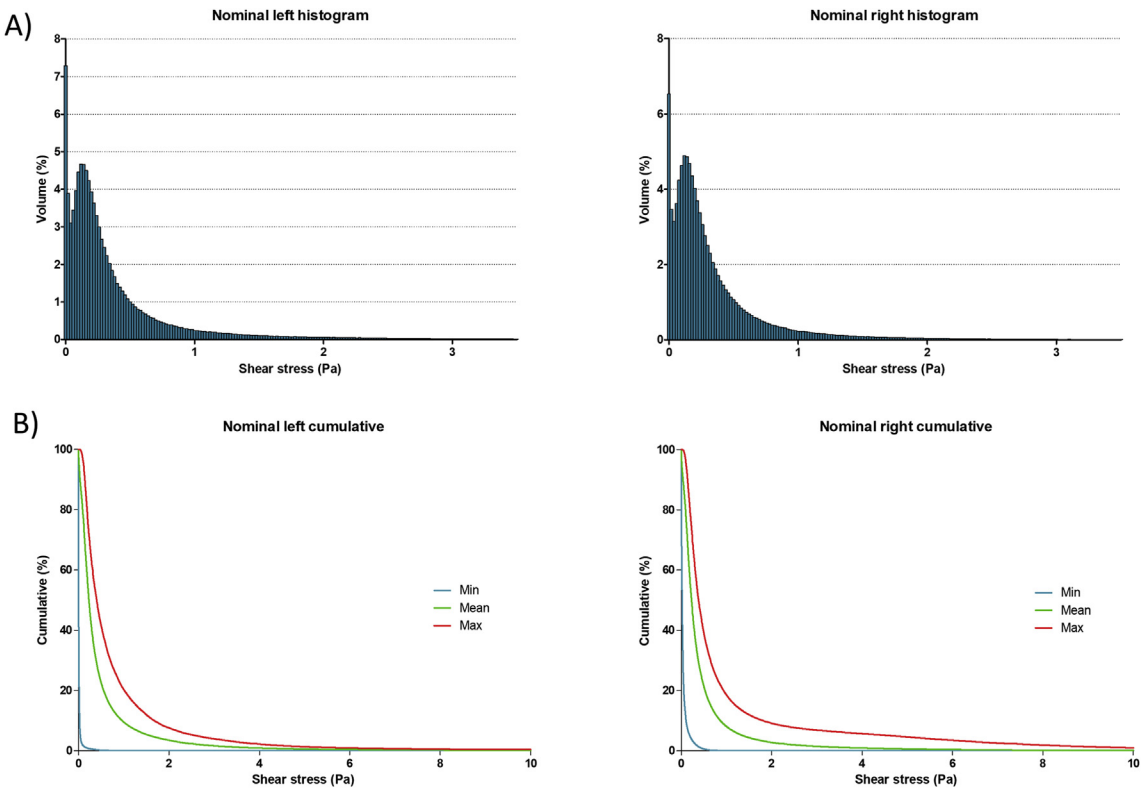

Figure 5. Simulation results. A: Histogram repartition of the shear stress (Pa) inside left ventricle and B: right ventricle occurring on one cycle of contraction at nominal pressure and flow. The Y-axis represents the percentage of blood volume, the X-axis the shear stress with a step of 0.02 Pa per column. C: Graph of the mean cumulated shear stress during one cycle of contraction in the left ventricle and D: right ventricle. The graph represents the envelop of the histogram repartition graph, The Y axis is the mean percentage of blood volume subject to a shear stress superior to the X axis corresponding value.

Table 2. Hemolysis and platelets activation simulated using CFD simulation.

Condition	Ventricle	Shear stress condition (Pa)	Hemolysis index (%)	Platelets activation index (%)
Contraction cycle (0.7 s)	Right	0.23	1.51×10^{-7}	3.10×10^{-4}
	Left	0.23	1.51×10^{-7}	3.10×10^{-4}
Systolic peak (0.2 s)	Right	3.75	3.38×10^{-5}	8.85×10^{-3}
	Left	3.71	3.31×10^{-5}	8.70×10^{-3}
	Estimated physiological value		5.8×10^{-4}	

and confirm the safety of the membrane through the aspects of aging, degradation, and impact on the blood stream elements.

The Carmat TAH design incorporates features, which mimic human circulatory characteristics. These comprise pulsatile flow, a viscoelastic pattern of contraction allowing for physiological pressure and flow waveforms, no areas of high shear stress and automatic physiological responses to preload variations. Continuous flow in the ventricular assist devices triggers hemodynamic issues [37] that can possibly be avoided using a pulsatile flow, because of the short exposure time to high shear stress. Clinical complications related to poor hemocompatibility, mainly associated to shear stress, have tempered the use of mechanical circulatory support and especially continuous flow pump, as a therapeutic option for patients suffering from end-stage heart failure. Absence of hemocompatibility has been largely attributed to shear stress inducing hemolysis, platelet activation and AWVS. This AWVS is prevalent in patients supported with LVAD [38, 39]. The high shear stresses induced by the LVADs trigger the unfolding of HMWM of vWF [28], and HMWM are sensible to a disintegrin and metalloprotease with thrombospondin type I repeats-13 (ADAMTS13) by cleavage [40, 41, 42]. The threshold of shear stress for unfolding the HMWM of vWF [28] is very close to the shear stress related to an observed increased activity of ADAMTS13 [29], thus a direct link exists between the shear stress applied and the cleavage activity of ADAMTS13 on HMWM of vWF [29]. Therefore, regarding potential degradation of vVWF after C-TAH implant, exposure to shears above 17.5 Pa is negligible according to the hemodynamic simulation, thus degradation by ADAMTS13 is negligible. These results were are in line with the absence of AVWS after C-TAH implantation in calves and humans [34, 36]. The thresholds set for the hemolysis and the platelets activations (150 Pa and 50 Pa, respectively) are commonly used to provide an order of magnitude for these phenomena, but are hardly not accurate. The 150 Pa threshold was set after studies of red blood cells degradation [43]. It is important to highlight the fact that the basic threshold was around 275 Pa, but sensitization protocol used to study the impact of long-term constant shear shifted this threshold to a significantly lower level of 150 Pa. The platelets activation threshold of 50 Pa was set after a review of different platelet activation experiments from the literature [25], and corresponds to the threshold for approximately 1 s of exposure. It is difficult to compare our results in hemolytic index and platelets activation for C-TAH to the results of the HM2 or the HeartWare (HW) [24] found in the literature, because the numerical simulation for these two devices uses Goubergrits approach [44]. First, the Goubergrits approach uses platelets lysis index, which is far less sensitive than platelets activation index. Secondly, even if this approach is interesting, it comes from *in-vitro* experiments obtained in the late 1980s, the results in the power laws seem far from what was observed more recently from blood in hemolysis [26] or platelets cytometry [27] and then less reliable. Thus, we chose to use equations to implement the time factor coming from in-vitro experiments that are more reliable than the only numerical simulation usually deployed. However, a comparison between the absolute shear stress values obtained from the simulations is possible. In a first study comparing HM2 and HW [24], 20% in the HM2 and 17% in the HW of blood volume undergoes shear stress superior to 9Pa. For shears >50Pa, approximatively 4% in the HM2 and 2.5% in the HW of

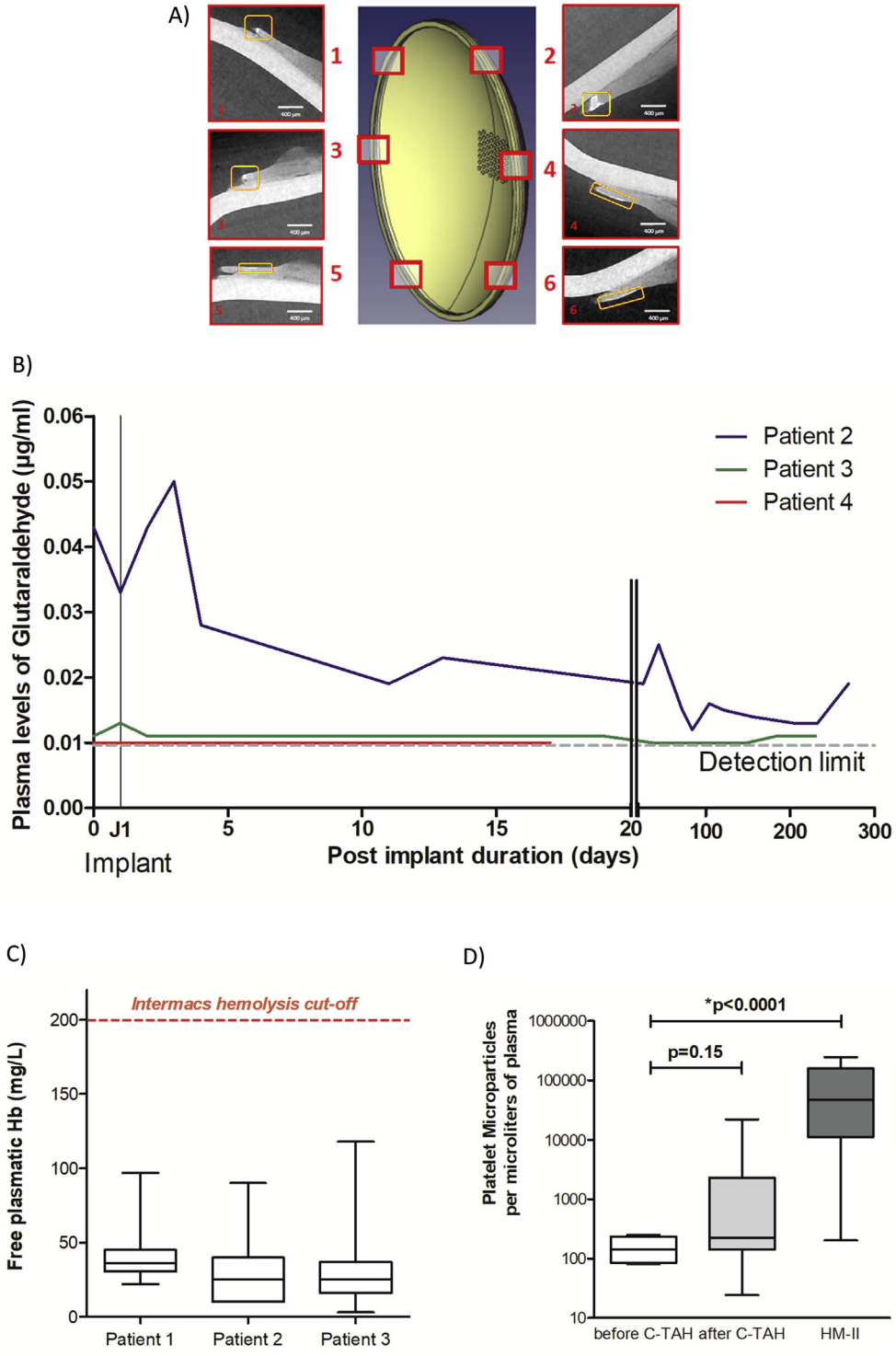

Figure 6. Results from feasibility clinical trial. A: 3D acquisition of the calcification for the hybrid membrane of the patient 3 of the clinical trial, with the corresponding views in cross sections, obtained by X-Ray micro-tomography. B: Plasma glutaraldehyde quantification before and after C-TAH implantation for the last three patients by LC-MS/MS. Values for patient 2 (blue), patient 3 (green) and patient 4 (red) are presented between pre-implant day and 269 days post implantation. C: Mean values of the plasma free hemoglobin for the first three patients after C-TAH implantation using spectrophotometry at specific wavelengths. D: Mean platelets microvesicles CD41 (in Annexin V positives MV) values for the first three patients of the clinical trial before (white) and after (light grey) C-TAH implantation, and compared to the values observed in five HeartMate II patients (dark grey).

the blood volume is concerned. In another study comparing HM2 vs HM3 [45], the number are slightly different for the HM2: 2.7% for shear stresses >50Pa vs 0.48% in HM3 and 0.09% in the HM2 for shear stresses >150Pa vs 0.03% in HM3. Nevertheless, in the C-TAH these values are at least 100 times lower: 0.13% of the volume for shear stresses >9Pa and less than 0.001% for left and 0.00015% for right ventricle regarding shear stresses >50Pa vs 0.48% in HM3 [45].

We confirmed here with data obtained in the three first implanted patients that C-TAH did not triggers hemolysis, significant platelets activation and already showed the absence of AVWS [34, 36], respectively by quantification of plasma free hemoglobin, platelets microvesicles and HMW multimers along follow-up. Thus, no biological perturbations related to shear stress in LVAD were present after C-TAH, confirming handling characteristics of C-TAH original design.

Currently, the total number of cardiac transplant worldwide is around 5,000 per each year and, for the 60–70 years old patients, the median survival is around 9 years after heart transplantation [46]. The C-TAH indications are bridge to transplantation and destination therapy, thus, one of the challenge in C-TAH implantation is to be a competitive tool compared to heart transplantation according to aging and longevity of

components. Aging tests demonstrated here that hybrid membrane separating oil compartment and the blood compartment is still intact after four 4 years of simulated aging. Exploration of erosion surface at the oil side was also studied in six membranes by Raman spectroscopy and surface topography. The ten membranes explored here in electronic microscopy showed no sign of deterioration. The mechanical degradation was not the only limit to the aging and to assess safety, the biological reaction triggered by the contact with the blood after implantation is also a factor of possible degradation, in particular for calcification. Thus we explored the efficiency of anti-calcification treatment in subcutaneous rat implantations. This animal model is commonly used for studying the biological reaction induced by implanted material [47, 48], including calcification. This test was successful in terms of calcification reduction and showed no significant toxicity of the material. In The X-Ray Micro tomography realized after a 9-month implantation of C-TAH in human confirmed this result since no area of calcification was detected in contact with blood. Micro calcification was observed at the periphery of the membrane, not in contact with blood or silicone oil. This peripheral calcification could result from the very low remnant glutaraldehyde quantity in the dead end, not accessible to the pre-operative washing, when in contact with plasma diffusion from the ventricular cavity, causing precipitation of the calcium due to the glutaraldehyde traces. As the area was not in contact with blood and not moving during the membrane displacement, there was no risk of embolism or change in the compliance of the hybrid membrane. Moreover, we performed plasma quantification of remnant glutaraldehyde after implantation, to ensure the absence of risk related to glutaraldehyde diffusion in plasma just after implantation, or to avoid any delayed diffusion from the dead end zone previously described. No significant increase of plasma quantification of remnant glutaraldehyde was observed after implantation or during the follow-up.

In conclusion, we demonstrated here the safety of the hybrid membrane regarding the mechanical aging, the calcification issues, and the impact of the membrane pulsatile movement on blood components. Safety confirmation of our findings will follow-up in the up-coming pivotal clinical study of the C-TAH (NCT02962973) implantation in 20 patients with end-stage biventricular heart failure.

Declarations

Author contribution statement

U. Richez: conceived and designed the experiments; performed the experiments; analyzed and interpreted the data; wrote the paper.

H. De Castilla: conceived and designed the experiments; performed the experiments; analyzed and interpreted the data.

C. Guerin: performed the experiments; analyzed and interpreted the data.

N. Gendron, C. Latremouille: performed the experiments.

G. Luraghi, M. Grimme, W. Wu, M. Taverna, P. Jansen, F. Migliavacca, G. Dubini, A. Carpentier: contributed reagents, materials, analysis tools or data.

A. Capel: conceived and designed the experiments; performed the experiments; contributed reagents, materials, analysis tools or data.

D. Smadja: conceived and designed the experiments; analyzed and interpreted the data; contributed reagents, materials, analysis tools or data; wrote the paper.

Funding statement

This work was supported by Carmat SA for clinical, preclinical study and also for lab reagents.

Competing interest statement

The authors declare the following conflict of interests: A. Carpentier is cofounder and shareholder of CARMAT SA. C. Latremouille and D.M. Smadja received consulting fees from CARMAT SA. U. Richez, P. Jansen and A. Capel are employed by CARMAT SA. U. Richez received a research grant from CARMAT SA.

Additional information

Supplementary content related to this article has been published online at https://doi.org/10.1016/j.heliyon.2019.e02914.

Acknowledgements

We thank medical and nursing staff of the cardiovascular intensive care unit and surgery departments involved in patient's follow-up. We also thank Brice Appenzeller from LIH (Luxembourg Institute of Health) for glutaraldehyde quantification in plasma.

References

[1] J.W. Rossano, A.I. Dipchand, L.B. Edwards, S. Goldfarb, A.Y. Kucheryavaya, B.J. Levvey, RN, L.H. Lund, B. Meiser, R.D. Yusen, J. Stehlik, The registry of the international society for heart and lung transplantation: nineteenth pediatric heart transplantation report—2016; focus theme: primary diagnostic indications for transplant, J. Heart Lung Transplant. 35 (2016) 1185–1195.

[2] S.A. Hunt, E.A. Rose, The REMATCH trial: long-term use of a left ventricular assist device for end-stage heart failure, Rev. Port. Cardiol. 20 (2001) 1279–1280.

[3] J.K. Kirklin, F.D. Pagani, R.L. Kormos, L.W. Stevenson, E.D. Blume, S.L. Myers, M.A. Miller, J.T. Baldwin, J.B. Young, D.C. Naftel, Eighth annual INTERMACS report: special focus on framing the impact of adverse events, J. Heart Lung Transplant. 36 (2017) 1080–1086.

[4] A. Carpentier, C. Latrémouille, B. Cholley, D.M. Smadja, J.C. Roussel, E. Boissier, J.N. Trochu, J.P. Gueffet, M. Treillot, P. Bizouarn, D. Méléard, M.F. Boughenou, O. Ponzio, M. Grimmé, A. Capel, P. Jansen, A. Hagège, M. Desnos, J.N. Fabiani, D. Duveau, First clinical use of a bioprosthetic total artificial heart: report of two cases, Lancet 386 (2015) 1556–1563.

[5] P. Jansen, W. van Oeveren, A. Capel, A. Carpentier, In vitro haemocompatibility of a novel bioprosthetic total artificial heart, Eur. J. Cardiothorac. Surg. 41 (2012).

[6] A. Carpentier, The surprising rise of nonthrombogenic valvular surgery, Nat. Med. 13 (2007) 1165–1168.

[7] H. Oxenham, P. Bloomfield, D.J. Wheatley, R.J. Lee, J. Cunningham, R.J. Prescott, H.C. Miller, Twenty year comparison of a Bjork-Shiley mechanical heart valve with porcine bioprostheses, Heart 89 (2003) 715–721. www.heartjnl.com. (Accessed 3 June 2019).

[8] K. Hammermeister, G.K. Sethi, W.G. Henderson, F.L. Grover, C. Oprian, S.H. Rahimtoola, Outcomes 15 years after valve replacement with a mechanical versus a bioprosthetic valve: final report of the Veterans Affairs randomized trial, J. Am. Coll. Cardiol. 36 (2000) 1152–1158.

[9] J.M. Brown, S.M. O'Brien, C. Wu, J.A.H. Sikora, B.P. Griffith, J.S. Gammie, Isolated aortic valve replacement in North America comprising 108,687 patients in 10 years: changes in risks, valve types, and outcomes in the Society of Thoracic Surgeons National Database, J. Thorac. Cardiovasc. Surg. 137 (2009) 82–90.

[10] ISO 14708-5:2010, Implants for Surgery – Active Implantable Medical Devices – Part 5: Circulatory Support Devices, 2019 n.d. https://www.iso.org/standard/52779.html.

[11] J. Lee, Long-term mechanical circulatory support system reliability recommendation by the national clinical trial initiative subcommittee, Am. Soc. Artif. Intern. Organs J. 55 (2009) 534–542.

[12] S.P. Sutera, M.H. Mehrjardi, Deformation and fragmentation of human red blood cells in turbulent shear flow, Biophys. J. 15 (1975) 1–10.

[13] S.P. Sutera, Flow-induced trauma to blood cells, Circ. Res. 41 (1977) 2–8. http://www.ncbi.nlm.nih.gov/pubmed/324656. (Accessed 27 February 2017).

[14] C.H. Brown, R.F. Lemuth, J.D. Hellums, L.B. Leverett, C.P. Alfrey, Response of human platelets to shear stress, ASAIO Journal, Am. Soc. Artif. Intern. Organs. 21 (1975) 35–39. http://journals.lww.com/asaiojournal/Citation/1975/21000/RESPONSE_OF_HUMAN_PLATELETS_TO_SHEAR_STRESS_.5.aspx. (Accessed 11 April 2017).

[15] S. Gogia, S. Neelamegham, Role of fluid shear stress in regulating VWF structure, function and related blood disorders, Biorheology 52 (2015) 319–335.

[16] U. Geisen, C. Heilmann, F. Beyersdorf, C. Benk, M. Berchtold-Herz, C. Schlensak, U. Budde, B. Zieger, Non-surgical bleeding in patients with ventricular assist devices could be explained by acquired von Willebrand disease, Eur. J. Cardiothorac. Surg. 33 (2008) 679–684.

[17] ISO 11357-1:2016, Plastics – Differential Scanning Calorimetry (DSC) – Part 1: General Principles, 2019 n.d. https://www.iso.org/standard/70024.html.

[18] ISO 9001:2015, Quality Management Systems – Requirements, 2019 n.d. https://www.iso.org/standard/62085.html.

[19] ISO 10993-1:2009, Biological Evaluation of Medical Devices – Part 1: Evaluation and Testing within a Risk Management Process, 2019 n.d. https://www.iso.org/standard/44908.html.

[20] European Parliament, Directive 2010/63/EU - on the protection of Animals Used for Scientific Purposes, 2010, 32010L0063.

[21] S.M. Carpentier, A.F. Carpentier, Double Cross-Linkage Process to Enhance post-implantation Bioprosthetic Tissue Durability, 2012. https://patents.google.com/patent/WO2012068241A2/e.https://patents.google.com/patent/WO2012068241A2/en (Accessed 8 April 2019).
[22] G. Luraghi, W. Wu, H. De Castilla, J.F. Rodriguez Matas, G. Dubini, P. Dubuis, M. Grimmé, F. Migliavacca, Numerical approach to study the behavior of an artificial ventricle: fluid–structure interaction followed by fluid dynamics with moving boundaries, Artif. Organs 42 (2018) E315–E324.
[23] G. Luraghi, W. Wu, F. De Gaetano, J.F. Rodriguez Matas, G.D. Moggridge, M. Serrani, J. Stasiak, M.L. Costantino, F. Migliavacca, Evaluation of an aortic valve prosthesis: fluid-structure interaction or structural simulation? J. Biomech. 58 (2017) 45–51.
[24] B. Thamsen, B. Blümel, J. Schaller, C.O. Paschereit, K. Affeld, L. Goubergrits, U. Kertzscher, Numerical analysis of blood damage potential of the HeartMate II and HeartWare HVAD rotary blood pumps, Artif. Organs 39 (2015) 651–659.
[25] K.H. Fraser, T. Zhang, M.E. Taskin, B.P. Griffith, Z.J. Wu, A quantitative comparison of mechanical blood damage parameters in rotary ventricular assist devices: shear stress, exposure time and hemolysis index, J. Biomech. Eng. 134 (2012), 081002.
[26] J. Ding, S. Niu, Z. Chen, T. Zhang, B.P. Griffith, Z.J. Wu, Shear-induced hemolysis: species differences, Artif. Organs 39 (2015) 795–802.
[27] J. Ding, Z. Chen, S. Niu, J. Zhang, N.K. Mondal, B.P. Griffith, Z.J. Wu, Quantification of shear-induced platelet activation: high shear stresses for short exposure time, Artif. Organs 39 (2015) 576–583.
[28] S.W. Schneider, S. Nuschele, A. Wixforth, C. Gorzelanny, A. Alexander-Katz, R.R. Netz, M.F. Schneider, Shear-induced unfolding triggers adhesion of von Willebrand factor fibers, Proc. Natl. Acad. Sci. U.S.A. 104 (2007) 7899–7903.
[29] S. Lippok, M. Radtke, T. Obser, L. Kleemeier, R. Schneppenheim, U. Budde, R.R. Netz, J.O. Rädler, Shear-induced unfolding and enzymatic cleavage of full-length VWF multimers, Biophys. J. 110 (2016) 545–554.
[30] C. Latrémouille, A. Carpentier, P. Leprince, J.C. Roussel, B. Cholley, E. Boissier, E. Epailly, A. Capel, P. Jansen, D.M. Smadja, A bioprosthetic total artificial heart for end-stage heart failure: results from a pilot study, J. Heart Lung Transplant. 37 (2018) 33–37.
[31] M.C. Menet, D. Gueylard, M.H. Fievet, A. Thuillier, Fast specific separation and sensitive quantification of bactericidal and sporicidal aldehydes by high-performance liquid chromatography: example of glutaraldehyde determination, J. Chromatogr. B Biomed. Appl. 692 (1997) 79–86.
[32] L. Goubergrits, K. Affeld, Numerical estimation of blood damage in artificial organs, Artif. Organs 28 (2004) 499–507.
[33] INTERMACS Adverse Event Definitions, Adult and Pediatric Patients, 2015, pp. 1–13. http://www.uab.edu/medicine/intermacs/images/protocol_4.0/protocol_4.0_MoP/Appendix_A_INTERMACS_AE_Definitions_Final_06122015.docx%5Cnhttp://www.uab.edu/medicine/intermacs/appendices-4-0/appendix-a-4-0.
[34] C. Latrémouille, D. Duveau, B. Cholley, L. Zilberstein, G. Belbis, M.F. Boughenou, D. Meleard, P. Bruneval, C. Adam, A. Neuschwander, J.C. Perles, P. Jansen, A. Carpentier, Animal studies with the carmat bioprosthetic total artificial heart, Eur. J. Cardiothorac. Surg. 47 (2015) e172–e179.
[35] D.M. Smadja, S. Susen, A. Rauch, B. Cholley, C. Latrémouille, D. Duveau, L. Zilberstein, D. Méléard, M.F. Boughenou, E. Van Belle, P. Gaussem, A. Capel, P. Jansen, A. Carpentier, The carmat bioprosthetic total artificial heart is associated with early hemostatic recovery and no acquired von Willebrand syndrome in calves, J. Cardiothorac. Vasc. Anesth. (2017).
[36] D.M. Smadja, B. Saubaméa, S. Susen, M. Kindo, P. Bruneval, E. Van Belle, P. Jansen, J.C. Roussel, C. Latrémouille, A. Carpentier, Bioprosthetic total artificial heart induces a profile of acquired hemocompatibility with membranes recellularization, J. Am. Coll. Cardiol. 70 (2017) 404–406.
[37] H. Patel, R. Madanieh, C.E. Kosmas, S.K. Vatti, T.J. Vittorio, Complications of continuous-flow mechanical circulatory support devices, Clin. Med. Insights Cardiol. 9 (2015) 15–21.
[38] A. Nascimbene, S. Neelamegham, O.H. Frazier, J.L. Moake, J.F. Dong, Acquired von Willebrand syndrome associated with left ventricular assist device, Blood 127 (2016) 3133–3142.
[39] N. Uriel, S.-W. Pak, U.P. Jorde, B. Jude, S. Susen, A. Vincentelli, P.-V. Ennezat, S. Cappleman, Y. Naka, D. Mancini, Acquired von Willebrand syndrome after continuous-flow mechanical device support contributes to a high prevalence of bleeding during long-term support and at the time of transplantation, J. Am. Coll. Cardiol. 56 (2010) 1207–1213.
[40] X. Zheng, D. Chung, T.K. Takayama, E.M. Majerus, J.E. Sadler, K. Fujikawa, Structure of von Willebrand factor-cleaving protease (ADAMTS13), a metalloprotease involved in thrombotic thrombocytopenic purpura, J. Biol. Chem. 276 (2001) 41059–41063.
[41] G.G. Levy, W.C. Nichols, E.C. Lian, T. Foroud, J.N. McClintick, B.M. McGee, A.Y. Yang, D.R. Siemieniak, K.R. Stark, R. Gruppo, R. Sarode, S.B. Shurin, V. Chandrasekaran, S.P. Stabler, H. Sabio, E.E. Bouhassira, J.D. Upshaw, D. Ginsburg, H.-M. Tsai, Mutations in a member of the ADAMTS gene family cause thrombotic thrombocytopenic purpura, Nature 413 (2001) 488–494.
[42] K. Soejima, N. Mimura, M. Hiroshima, H. Maeda, T. Hamamoto, T. Nakagaki, C. Nozaki, A novel human metalloprotease synthesized in the liver and secreted into the blood: possibly, the von Willebrand factor–cleaving protease? J. Biochem. 130 (2001) 475–480.
[43] O.K. Baskurt, H.J. Meiselman, Red blood cell mechanical stability test, Clin. Hemorheol. Microcirc. 55 (2013) 55–62.
[44] L. Goubergrits, Numerical Modeling of blood damage: current status, challenges and future prospects, Expert Rev. Med. Devices 3 (2006) 527–531.
[45] K. Bourque, C. Cotter, C. Dague, D. Harjes, O. Dur, J. Duhamel, K. Spink, K. Walsh, E. Burke, Design rationale and preclinical evaluation of the HeartMate 3 left ventricular assist system for hemocompatibility, Am. Soc. Artif. Intern. Organs J. 62 (2016) 375–383.
[46] R.D. Yusen, L.B. Edwards, A.I. Dipchand, S.B. Goldfarb, A.Y. Kucheryavaya, B.J. Levvey, L.H. Lund, B. Meiser, J.W. Rossano, J. Stehlik, The registry of the international society for heart and lung transplantation: thirty-third adult lung and heart–lung transplant report—2016; focus theme: primary diagnostic indications for transplant, J. Heart Lung Transplant. 35 (2016) 1170–1184.
[47] W.J. Mako, I. Vesely, In vivo and in vitro models of calcification in porcine aortic valve cusps, J. Heart Valve Dis. 6 (1997) 316–323. http://www.ncbi.nlm.nih.gov/pubmed/9183732. (Accessed 3 January 2017).
[48] L.J. Quintero, J.M. Lohre, N. Hernandez, S.C. Meyer, T.J. McCarthy, D.S. Lin, S.H. Shen, Evaluation of in vivo models for studying calcification behavior of commercially available bovine pericardium, J. Heart Valve Dis. 7 (1998) 262–267. https://www.ncbi.nlm.nih.gov/labs/articles/9651837/. (Accessed 3 January 2017).